THE JOURNAL OF PHYSICAL CHEMISTRY C

Article

pubs.acs.org/JPCC

# Atomistic Modeling of Sulfur Vacancy Diffusion Near Iron Pyrite Surfaces

Y. N. Zhang,*[,†,‡,§] M. Law,[‖] and R. Q. Wu[§]

[†]Chengdu Green Energy and Green Manufacturing Technology R&D Center, Chengdu, Sichuan 610207, China

[‡]Beijing Computational Science Research Center, Beijing, 100084, China

[§]Department of Physics and Astronomy, University of California, Irvine, California 92697, United States

[‖]Department of Chemistry, University of California, Irvine, California 92697, United States

**ABSTRACT:** Through density functional calculations, we investigated the diffusion of isolated sulfur vacancies ($V_S$) from the bulk of iron pyrite (cubic $FeS_2$) to the (100) and (111) surfaces. The influence of vacancy depth on the vacancy formation energy and the activation energy for vacancy diffusion are discussed. Significantly, we find that $V_S$ defects tend to migrate toward stoichiometric and sulfur-rich surfaces through sequential "intra-dimer" and "inter-dimer" hops. We find a pre-exponential constant ($D_0$) of $9 \times 10^{-7}$ m$^2$ s$^{-1}$ and an activation energy ($E$) of 1.95 eV for sulfur vacancy diffusion in bulk pyrite, corresponding to a vacancy diffusion coefficient $D_V = D_0 \exp(-E/kT) = 9 \times 10^{-40}$ m$^2$ s$^{-1}$ at 25 °C and $5 \times 10^{-18}$ m$^2$ s$^{-1}$ at 600 °C. The activation energy is smaller near the surface (e.g., $E$ = 1.5 eV near the stoichiometric (100) surface), resulting in faster vacancy diffusion near the surface than in the bulk. Using the formation enthalpy of $V_S$ at the (100) surface, $E$ = 2.37 eV, we find a sulfur diffusivity in bulk pyrite $D_S = 7 \times 10^{-47}$ m$^2$ s$^{-1}$ at 25 °C and $2 \times 10^{-20}$ m$^2$ s$^{-1}$ at 600 °C. The calculated $D_S$ values are in reasonable agreement with experiment only at intermediate temperatures (~275−625 °C). Our results show that bulk and near-surface sulfur vacancies can be healed in sulfur-rich conditions at reasonably high temperatures. The mechanism of vacancy diffusion presented here should be useful in managing $V_S$ defects during the fabrication of high-quality pyrite samples for solar energy conversion applications.

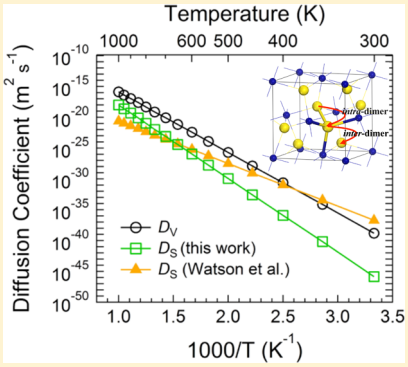


## 1. INTRODUCTION

The control of point defects in solids is a crucial issue for the optimal performance of many materials, including semiconductors,[1−6] high-$\kappa$ dielectrics,[7−9] and steels.[10,11] Iron pyrite ($FeS_2$) is a promising semiconductor for use in photovoltaic and photoelectrochemical cells due to its suitable band gap, excellent optical absorptivity, and essentially infinite abundance of iron and sulfur in the planet's crust.[12] The main hurdle for the development of pyrite solar cells is its unexpectedly low conversion efficiency, ~3%, which is primarily due to the low open circuit voltage, $V_{OC} \approx 200$ meV.[13,14] Electronic states produced by surfaces and bulk defects are often identified as the ultimate source of the low $V_{OC}$.[15−18] In addition, ab initio simulations show that some defects may reduce the band gap of pyrite and hence degrade its photovoltaic performance.[19−24] Fe vacancies ($V_{Fe}$) and S vacancies ($V_S$) are among the simplest point defects in pyrite. Despite the relatively high formation energy of $V_S$ predicted by several recent density functional theory (DFT) studies (2.27−2.7 eV under sulfur-poor conditions, which implies a negligible equilibrium $V_S$ concentration),[19,21,22,25,26] a high concentration of sulfur vacancies has been reported using techniques such as high resolution X-ray diffraction (HRXRD),[27] photoemission of adsorbed Xe (PAX),[28,29] scanning tunneling microscopy (STM),[30] and atomic emission spectroscopy (AES).[31,32] Furthermore, the stoichiometry of pyrite samples has been found to change significantly with temperature and surface conditions.[33−38] Therefore, it is crucial to optimize the processing conditions for the removal of sulfur vacancies in pyrite films, starting from an understanding of the diffusion mechanism of individual vacancies near the surface.

The calculated surface energies of stoichiometric pyrite surfaces increase in the order (100) < (111) < (210) < (110).[39] These four surfaces are commonly observed in experiments, for example, in the growth of macroscopic single crystals[18,40] and shape-controlled nanocrystals.[41,42] In this paper, we report DFT results of sulfur vacancy diffusion near the (100) and (111) surfaces as a function of surface stoichiometry. Our results show that sulfur vacancies tend to diffuse toward the surface for all the cases studied here, with potential energy profiles that depend strongly on the surface stoichiometry.

## 2. COMPUTATIONAL METHODOLOGY

As sketched in Figure 1a, pyrite $FeS_2$ adopts a NaCl-like structure, with a face-centered cubic sublattice of diamagnetic $Fe^{2+}$ ions and ⟨111⟩-oriented $S_2^{2-}$ dimers occupying the anion positions.[22] Each Fe ion is octahedrally coordinated to six S ions, and each S ion has three Fe neighbors and one S neighbor.

**Received:** August 26, 2015
**Revised:** September 9, 2015




DOI: 10.1021/acs.jpcc.5b08300
J. Phys. Chem. C XXXX, XXX, XXX−XXX

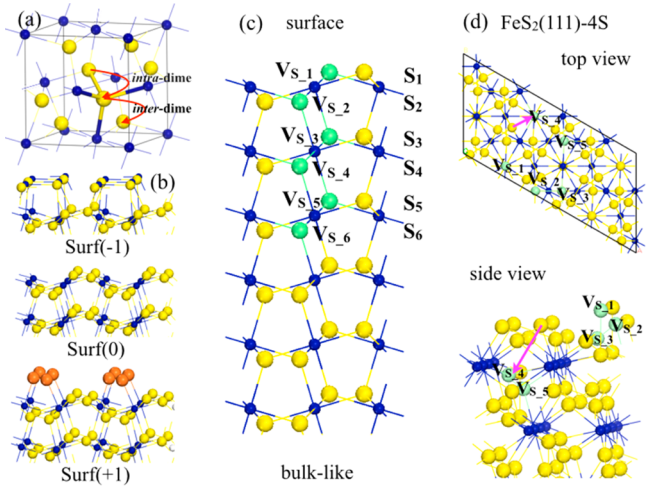


**Figure 1.** (a) Bulk unit cell of pyrite $FeS_2$ and a sketch of intradimer and interdimer $V_S$ hops during vacancy diffusion. Yellow and blue spheres represent S and Fe atoms, respectively. (b) Relaxed structures of the three $FeS_2(100)$ surfaces explored in this study. The large orange spheres represent the additional sulfur atoms added to the stoichiometric surface, Surf(0). (c) Schematic diagram of single sulfur vacancies (green spheres labeled $V_{S\_n}$) in each of the n layers of Surf(0). This shows a (010) projection of the (100) surface. (d) Top and side views of the $FeS_2(111)$-4S surface. $V_{S\_1}$-$V_{S\_5}$ are the various positions of sulfur vacancies near the surface. The pink arrow shows the hopping of a neighboring sulfur atom to $V_{S\_4}$.

The cleavage of pyrite typically leads to a complex surface morphology and stoichiometry. For example, cleavage of only the Fe−S bonds perpendicular to a (100) plane creates the stoichiometric (100) surface, whereas mixed cleavage of S−S and Fe−S bonds creates various nonstoichiometric surfaces.[23] Here, we use three different surface stoichiometries to produce different environments for the diffusion of $V_S$ near the (100) surface, as shown in Figure 1b. Our previous DFT studies have shown that these three surfaces are thermodynamically stable in $SO_2$-rich, $H_2S$-rich, and S-rich conditions, respectively.[23] We used a periodic slab of 11 $FeS_2$ atomic layers and a vacuum layer 17 Å thick to model $V_S$ diffusion near the (100) surfaces. Our previous work shows that this 11-layer slab model is sufficiently thick to reproduce the physical and electronic structure of bulk pyrite in the middle layers.[23] The slabs were constructed with two identical surfaces in order to avoid artificial electric fields in the vacuum during studies of polar surfaces. A (2 × 2) lateral supercell was used with one sulfur ion removed from a specific sulfur layer. In this paper, we denote a sulfur atom in the *n*th sulfur atomic layer as S_*n* (*n* = 1−6) and a sulfur vacancy in this layer as $V_{S\_n}$, as depicted in Figure 1c.

The $FeS_2(111)$ surface is more complex, with five different surface terminations. One surface is Fe-terminated and the others contain 1−4 layers of S ions (denoted by (111)-Fe, (111)-S, (111)-2S, (111)-3S, and (111)-4S, respectively, cf., Figure 5 in ref 39.). Here, we performed calculations for the stoichiometric (111)-2S, and S-rich (111)-3S and -4S surfaces. A periodic hexagonal slab model with nine $FeS_2$ atomic layers and a vacuum layer 18 Å thick was used. To simulate a similar vacancy concentration as for the (100) surface, we adopted a (2 × 1) lateral supercell with more than 230 atoms, as depicted in Figure 1d.

Spin-polarized density functional calculations were performed using the Vienna Ab initio Simulation Package (VASP)[43] with the projector augmented wave (PAW) method.[44] The generalized gradient approximation (GGA)[45] was adopted to describe the exchange-correlation interaction among electrons, and a Hubbard U of 2 eV was added for Fe 3d orbitals.[23,46,47] We used an energy cutoff of 350 eV for the plane-wave basis expansion. The convergence of our results against the number of *k*-points in the Brillouin zone was carefully monitored in each case. The lattice constant in the lateral plane was fixed at the optimized value for bulk pyrite, $a$ = 5.422 Å. The Fe and S atoms in the central layer were fixed at their bulk positions, whereas all other atoms were fully relaxed until forces on them became smaller than 0.01 eV/Å.

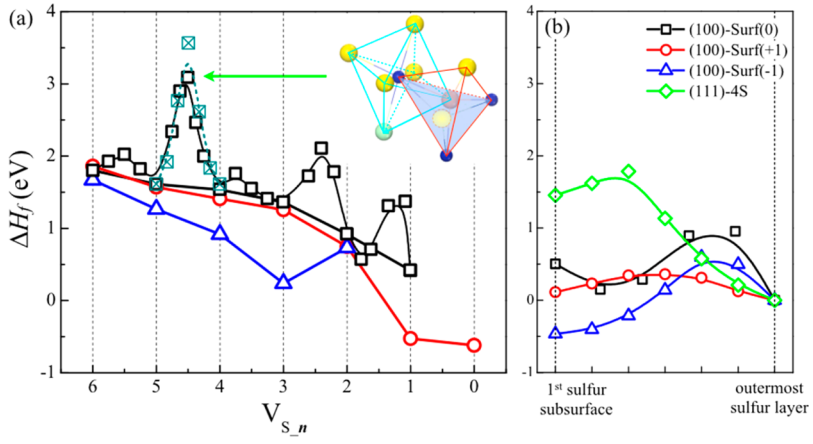


**Figure 2.** (a) Vacancy formation energy, $\Delta H_f$, as a function of vacancy depth for $FeS_2(100)$ surfaces with three different stoichiometries. The black squares show the full potential energy profile (including energy barriers for each hop) for Surf(0). The energy barrier of the "*inter*-dimer" motion in bulk pyrite is indicated with dark cyan crossed squares. The inset is the atomic structure of the $V_{S\_5} \leftrightarrow$ S_4 transition state (highlighted by the green arrow). The yellow and blue spheres denote S and Fe atoms. The green and orange spheres represent the vacancy and migrating sulfur atom, respectively. (b) Potential energy profiles for $V_S$ hopping between the first subsurface sulfur layer and the outermost sulfur layer of the three (100) surfaces and the (111)-4S surface. The profiles correspond to $V_{S\_3} \leftrightarrow$ S_2 for Surf(−1), $V_{S\_2} \leftrightarrow$ S_1 for Surf(0), $V_{S\_1} \leftrightarrow$ S_0 for Surf(+1), and $V_{S\_4} \leftrightarrow$ S_2 for (111)-4S surfaces. The data are plotted relative to the enthalpies of a $V_S$ on each outermost sulfur layer.



DOI: 10.1021/acs.jpcc.5b08300
J. Phys. Chem. C XXXX, XXX, XXX−XXX

## 3. RESULTS AND DISCUSSION

To annihilate a sulfur vacancy in bulk pyrite, it is conceivable that sulfur atoms could move from the surface through the crystal by interstitial diffusion, i.e., hopping through the unoccupied tetrahedral interstitial sites in the FCC Fe lattice. However, our calculations show that the formation energy of a sulfur interstitial is prohibitively high (>8 eV) for this mechanism to occur.[22] The calculated activation energy for sulfur interstitial diffusion is also very high. For example, a sulfur atom at Surf(+1) moving from the topmost layer to $V_{S\_6}$ needs to overcome energy barriers as large as 4.1 eV. Given typical annealing temperatures,[48,49] it is very unlikely that $V_S$ centers are healed in this direct way. Instead, we believe that vacancy diffusion, i.e., sequential hopping of sulfur atoms into a vacancy leading to migration of the vacancy through the crystal and eventually to the surface, is the most reasonable mechanism of $V_S$ annihilation.

To determine the feasibility of vacancy diffusion, we calculated the position dependence of the formation enthalpy of $V_S$ according to

$$\Delta H_f = E_{vac} - E_{perf} + \mu_S \quad (1)$$

Here, $E_{vac}$ and $E_{perf}$ are the energies of surface slabs with and without vacancies, respectively. The chemical potential of one S atom, $\mu_S$, is a parameter to simulate the change of environment from oxidizing conditions to S-rich conditions (e.g., $\mu_S = -6.32$ eV in $SO_2$ and $\mu_S = 0$ for an isolated sulfur atom). Using $\mu_S = -3.77$ eV, which corresponds to sulfur-poor conditions, the calculated vacancy formation energies at the three (100) surfaces are shown in Figure 2 as a function of the $V_S$ depth. Clearly, $\Delta H_f$ decreases as the vacancy moves from the bulk to the surface, indicating that bulk vacancies have an energetic driving force for diffusing toward the surface. This is understandable since it is easier for surface atoms than bulk atoms to adjust their positions and charge states to accommodate the vacancy. The only exception is for Surf(−1), where the calculated $\Delta H_f$ of $V_{S\_2}$ is higher than that of $V_{S\_3}$ by 0.4 eV. In this case, the vacancy is likely to be trapped in subsurface layer S_3 instead of moving to the topmost S_2 layer that is already sulfur poor. The calculated $\Delta H_f$ for $V_{S\_1}$ of Surf(0) is only 0.42 eV, much lower than $\Delta H_f$ = 2.36 eV for bulk pyrite under the same sulfur-poor conditions. Accordingly, the vacancy density at the surface should be rather high, particularly under weakly oxidizing growth or annealing conditions. The calculated equilibrium vacancy concentration, $[V_S]$, which is determined by $[V_S] = [V_S]_{max}\exp(-\Delta H_f/k_BT)$ with $[V_S]_{max} = 5 \times 10^{22}$ cm$^{-3}$, changes from $3 \times 10^{-8}$ cm$^{-3}$ for $V_{S\_6}$ to $5 \times 10^{15}$ cm$^{-3}$ for $V_{S\_1}$ at Surf(0) at room temperature. At typical synthesis/annealing temperatures of 300−600 °C, the expected vacancy concentration becomes $10^7$−$10^{13}$ cm$^{-3}$ in the bulk and $10^{19}$−$10^{20}$ cm$^{-3}$ near the surface. Note that for the same sulfur chemical potential, $\Delta H_f$ for $V_{S\_0}$ in Surf(+1) becomes negative (−0.62 eV), as shown by the red circles in Figure 2, indicating spontaneous formation of $V_{S\_0}$ at Surf(+1). This is consistent with our previous study that showed that Surf(+0.875) has a lower surface energy than Surf(+1) at $\mu_S = -3.77$ eV.[23] It is known that Surf(0) is the most stable (100) surface in the range of $-3.85$ eV $< \mu_S < -3.17$ eV and that Surf(+1) is stable over a large range of $\mu_S$ in sulfur-rich conditions, with a lower surface energy than a Surf(+1) + Vs surface. Therefore, we believe that the continuous diffusion of $V_S$ to the surface will not affect the surface stoichiometry of pyrite samples that are immersed in a sulfur reservoir with a fixed $\mu_S$.

While the diffusion of $V_S$ toward the surface is energetically favorable, the energy barriers along the various possible trajectories govern the kinetics of this diffusion process. We calculated the potential energy profile for vacancy diffusion from the bulk to Surf(0) (Figure 2). To determine the lowest-energy trajectory for vacancy motion, we moved the neighboring sulfur atom toward the vacancy along the surface normal in 0.3 Å steps and, at each step, allowed the lateral positions of all atoms to relax until forces on them became smaller than 0.01 eV/Å. We find an energy barrier of only 0.23 eV for $V_{S\_6}$ hopping into S_5. This low barrier is understandable given that these two sites belong to the same original S−S dimer. Indeed, at equilibrium the S_5 atom of the original dimer is displaced 0.16 Å toward the $V_{S\_6}$ site relative to its position in the perfect crystal, while displacement of the surrounding Fe atoms is negligible. Bader charge analyses show that, while the charge state of Fe atoms remain unchanged (+0.88 e), the charge of the S_5 atom near $V_{S\_6}$ becomes −0.80 e, almost double that of a sulfur ion in the perfect crystal. This charge distribution is very similar for an isolated $V_S$ center in bulk pyrite.[22] Overall, the "*intra*-dimer" vacancy hop depicted in Figure 1a appears to be quite facile, even at room temperature.

Next, we calculated the barrier for the motion of a vacancy to an adjacent S−S dimer, i.e., the "*inter*-dimer" vacancy hop sketched in Figure 1a. This hop involves the movement of an S atom from its normal $SFe_3$ tetrahedral coordination and across the intervening (111) plane of hexagonal packed Fe atoms to reach the vacancy. Our results show that the lowest-energy path involves an S atom moving from its lattice site in a ⟨111⟩ direction, passing almost exactly through the center of the $Fe_3$ triangle of its original coordination polyhedron, and then turning to move directly to the $V_S$ site, tracing an overall bent trajectory. We find an energy barrier of 1.5 eV for $V_{S\_5}$ hopping into S_4 (Figure 2a), suggesting that *inter*-dimer vacancy hopping is rate limiting and that fairly high temperatures are needed to activate diffusion. This value is significantly smaller than the calculated barrier of 1.95 eV for the same process in the crystal bulk, as shown in Figure 2a (crossed squares). Interestingly, we found that the energy barrier for a positively charged sulfur vacancy in a $(2 \times 2 \times 2)$ bulk pyrite supercell drops to 1.91 eV, and is slightly lower in a larger $(3 \times 3 \times 3)$ supercell when atoms have more rooms to relax in the transition state. So, we can expect the activation energy for diffusion in real samples to be lower than the values calculated here when charged defects are present. The structure of the $V_{S\_5} \leftrightarrow$ S_4 transition state is illustrated as a representative example in the inset of Figure 2a. In the transition state, the migrating S atom (orange sphere) has moved out of its $SFe_3$ coordination polyhedron (red tetrahedron) to nearly the center of the $Fe_3$ triangle (shaded blue) that separates it from the vacancy (green sphere). Note that the high barrier for sulfur diffusion is not due to strain, since the triangle of Fe ions is large enough for the sulfur atom to pass through ($d_{S-Fe}$ = 2.25−2.49 Å). Rather, the main cause for the high activation energy is the cleavage of the S−S dimer. The S−S bond length in the transition state increases from 2.16 to 2.58 Å. The transition state in the bulk crystal is very similar. We conclude that "*inter*-dimer" vacancy hops determine the rate of vacancy diffusion in the bulk and toward the surface of pyrite.

Strikingly, the energy barriers for both *intra*- and *inter*-dimer hopping gradually decrease near the Surf(0) surface because of


DOI: 10.1021/acs.jpcc.5b08300
J. Phys. Chem. C XXXX, XXX, XXX−XXX

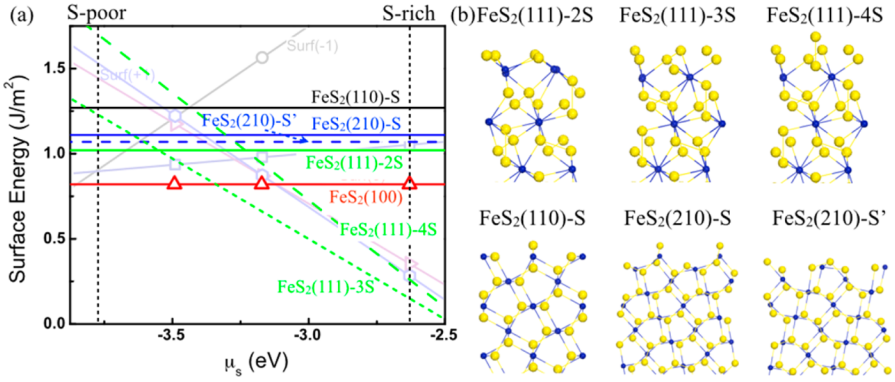


**Figure 3.** (a) Calculated surface energies of different $FeS_2$(111), (110), and (210) surfaces versus the sulfur chemical potential, $\mu_S$. (b) Corresponding optimized structures. The yellow and blue spheres represent S and Fe atoms, respectively.

the greater freedom of near-surface atoms to adjust their positions and charge states to accommodate the vacancy. In particular, the energy barrier of the final step, $V_{S\_2} \rightarrow S\_1$ (conversely, the initial step for sulfur atoms to enter the crystal), is only 0.8 eV. It is also worthwhile to point out that the energy barriers are strongly biased in favor of vacancy diffusion toward the surface due to the monotonic decrease of $\Delta H_f$ near the surface. For example, the inward hop $V_{S\_2} \rightarrow S\_3$ has an energy barrier of 1.6 eV, much higher than 0.8 eV for the outward hop. Thus, the potential energy profile effectively frustrates the formation of new $V_S$ centers in the crystal bulk and suggests that $V_S$ defects accumulate in the near-surface region of pyrite. To explore the effects of surface conditions, we also calculated the energy barriers for the final $V_S$ hop between the first subsurface sulfur layer and outermost sulfur layer of Surf(−1) and Surf(+1) (that is, $V_{S\_3} \rightarrow S\_2$ for Surf(−1) and $V_{S\_1} \rightarrow S\_0$ for Surf(+1)). The resulting potential profiles plotted in Figure 2b show that the energy barrier for $V_S$ diffusion to the outermost layer of Surf(+1) is only 0.25 eV. Therefore, excess sulfur atoms can easily diffuse into the subsurface to annihilate vacancies when the surface is sulfur-rich. In contrast, the corresponding barrier for Surf(−1) is ∼1.1 eV (compared to only 0.7 eV for inward vacancy diffusion). Therefore, we can expect a high $V_S$ density in the subsurface layer of Surf(−1) and diffusion of sulfur into the crystal is slowed. Our results confirm that sulfur-rich conditions on the $FeS_2$(100) surface should be beneficial for the removal of $V_S$ defects.

To see if the same outward diffusion tendency of $V_S$ is true of other surfaces, we performed calculations for three $FeS_2$(111) surfaces and the stoichiometric (110) and (210) surfaces. We first identified the most probable surface morphologies by calculating their surface energies at temperature $T$ and pressure $p$ according to the equation

$$\gamma(T, p) = \frac{1}{2A}[G(T, p, N_{Fe}, N_S) - N_{Fe}\mu_{Fe}(T, p) - N_S\mu_S(T, p)] \quad (2)$$

Here, $A$ is the surface area, $G(T, p, N_{Fe}, N_S)$ is the Gibbs free energy of the slab, and $N_{Fe}$ and $N_S$ are the numbers of Fe and S atoms. We applied a constraint that requires the chemical potentials of Fe ($\mu_{Fe}$) and S ($\mu_S$) to obey $\mu_{Fe} + 2\,\mu_S = \mu_{FeS2}$, where $\mu_{FeS2}$ is the chemical potential of one $FeS_2$ formula unit in bulk pyrite. Under ambient conditions, $G$ can be approximated by the total energy without contributions from configurational or vibrational entropy.

The calculated surface energies of several $FeS_2$(111), (110), and (210) surfaces are shown in Figure 3, along with the corresponding atomic configurations. Here, values of $\mu_S$ range from the energy of a sulfur atom in $H_2S$ (−3.77 eV) to that of a sulfur atom in $S_2$ (−2.63 eV) to simulate sulfur-poor to sulfur-rich conditions. We see that the stoichiometric $FeS_2$(100) surface has the lowest surface energy in sulfur-poor conditions, whereas the sulfur-rich $FeS_2$(111)-3S and 4S surfaces are more stable than others in the S-rich side. This is consistent with our experimental observations and previous DFT studies.[39,50] Taking the $FeS_2$(111)-4S surface as an example, we studied the diffusion of $V_S$ near the surface, and found that the vacancy formation energies decrease from $V_{S\_5}$ to $V_{S\_1}$ because, again, near-surface atoms can relax more easily. Since $\Delta H_f$ is small, for example, 0.53 eV for $V_{S\_4}$ at the (111)-4S surface under the condition $\mu_S$ = 3.77 eV, we expect the population of $V_S$ near (111) surfaces to also be high in as-grown samples. Since the calculated energy barrier for $V_{S\_4} \rightarrow S\_2$, as highlighted by the pink arrow in Figure 1d and plotted in Figure 2b, is only 0.33 eV, sulfur vacancies near the (111) surface should be easily expelled under sulfur-rich conditions.

Perhaps the most important experimental quantities that can be calculated from our results are the diffusion coefficients for sulfur vacancies ($D_V$) and sulfur atoms ($D_S$) in bulk pyrite. $D_V$ is proportional to the product of the average number of interdimer sulfur atoms adjacent to a vacancy and the $S_S$-to-$V_S$ hopping rate, i.e., $D_V = \alpha[1 - \exp(-\Delta H_f/k_BT)]g\nu d^2\exp(-E_a/k_BT)$. For sulfur self-diffusion by the vacancy mechanism, $D_S$ is proportional to the product of the average number of vacancies adjacent to a sulfur atom and the $S_S$-to-$V_S$ hopping rate, i.e., $D_S = \alpha \exp(-\Delta H_f/k_BT)g\nu d^2 \exp(-E_a/k_BT)$.[51] Here, $\alpha$ is the number of interdimer sulfur nearest neighbors for a sulfur atom in pyrite ($\alpha$ = 6), $\Delta H_f$ is the vacancy formation energy, $g$ is a geometric factor ($g$ = 1/6 for 3D diffusion), $\nu$ is the attempt frequency, $d$ is the hopping distance, $E_a$ is the activation energy for a $S_S$-$V_S$ hop, $k_B$ is Boltzmann's constant, and $T$ is the temperature. The diffusivity expression is often simplified to $D = D_0 \exp(-E/k_BT)$, where $D_0 = \alpha g\nu d^2$ is the pre-exponential constant and $E$ is the overall activation energy for diffusion, with $E \approx E_a$ for vacancy diffusion and $E = \Delta H_f + E_a$ for sulfur self-diffusion. Here, $d$ = 3.06 Å is the shortest distance between $V_S$ and $S_S$ of a neighboring dimer. The attempt frequency, $\nu$, was determined by calculating the vibrational frequency of the migrating sulfur atom using the linear response approach. We find $\nu \sim 10^{13}$ $s^{-1}$ for sulfur atoms vibrating at their equilibrium sites and, accordingly, $D_0 \approx 9 \times 10^{-7}$ $m^2$ $s^{-1}$.



DOI: 10.1021/acs.jpcc.5b08300
J. Phys. Chem. C XXXX, XXX, XXX−XXX

Figure 4 plots $D_V$ and $D_S$ for bulk pyrite as a function of temperature. Since $\Delta H_f$ is large (>0.4 eV), sulfur atoms hugely

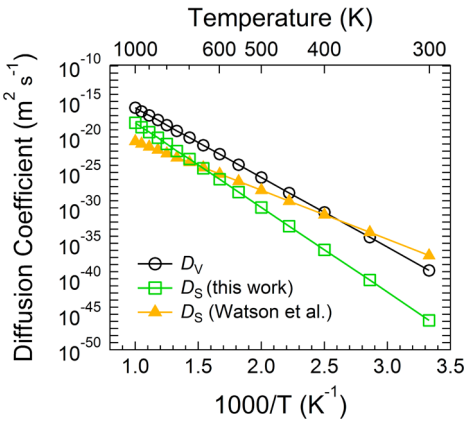


**Figure 4.** Calculated diffusion coefficients for sulfur vacancies ($D_V$) and sulfur atoms ($D_S$) in bulk pyrite as a function of temperature. Experimental $D_S$ data from ref 52 are shown for comparison.

outnumber vacancies and $D_V \gg D_S$ at all experimentally relevant temperatures. In other words, vacancies move faster than sulfur atoms because each vacancy is always surrounded by ~6 sulfur atoms, while the probability for a sulfur atom to have an adjacent vacancy is very low. Using $E_a$ = 1.95 eV, we find $D_V = 9 \times 10^{-40}$ m$^2$ s$^{-1}$ at 25 °C and $5 \times 10^{-18}$ m$^2$ s$^{-1}$ at 600 °C. Vacancy diffusion is significantly faster within 1 nm of the surface (e.g., $D_V = 4 \times 10^{-32}$ m$^2$ s$^{-1}$ at 25 °C near the (100) surface). It is of course expected that both surface and near-surface diffusion are faster than bulk diffusion.

Unlike $D_V$, $D_S$ depends critically on the value of $\Delta H_f$. If we use the bulk value of $\Delta H_f$ in sulfur-poor conditions (2.36 eV), we have $E = \Delta H_f + E_a$ = 4.31 eV, and an extraordinarily low sulfur diffusivity, $D_S = 1 \times 10^{-79}$ m$^2$ s$^{-1}$ at 25 °C. If we instead use the value of $\Delta H_f$ at the surface (e.g., $\Delta H_f$ = 0.42 eV at Surf(0))—appropriate if vacancies form mainly at the surface during nonequilibrium crystal growth and are then buried within the growing crystal, which seems likely—then $E$ = 2.37 eV and $D_S = 7 \times 10^{-47}$ m$^2$ s$^{-1}$ at 25 °C and $2 \times 10^{-20}$ m$^2$ s$^{-1}$ at 600 °C (Figure 4). Watson et al. have reported on sulfur self-diffusion experiments using natural pyrite single crystals.[52] Based on fitting $^{34}$S diffusion profiles of (100) crystals immersed in liquid $^{34}$S at 500–725 °C, these authors found $D_S = (2 \times 10^{-14}\ \text{m}^2\ \text{s}^{-1}) \exp(-1.37\ \text{eV}/k_BT)$, which gives $D_S = 1 \times 10^{-37}$ m$^2$ s$^{-1}$ at 25 °C and $2 \times 10^{-22}$ m$^2$ s$^{-1}$ at 600 °C (Figure 4). Our calculated $D_S$ values are thus in reasonable agreement with experiment only if vacancies form at the crystal surface (where $\Delta H_f$ is relatively small) and are then trapped in the bulk, or if the bulk vacancy concentration is otherwise much higher than its calculated equilibrium value (possibly because $V_S$ forms in association with another defect). However, the agreement between experiment and theory seen at intermediate temperatures (~275–625 °C) in Figure 4 is fortuitous, since the experimental values of $D_0$ and $E$ are both significantly smaller than predicted here. Future work is needed to evaluate whether sulfur self-diffusion in real pyrite samples readily occurs by mechanisms other than simple vacancy diffusion.

In summary, we performed systematic density functional calculations to understand the mechanism and determine the diffusion coefficient of sulfur vacancy diffusion near different pyrite surfaces. Formation energy calculations reveal that near-surface sulfur vacancies tend to move toward the surface via sequential "*intra*-dimer" and "*inter*-dimer" hopping, with the latter determining the rate of vacancy diffusion. We find an expression for the bulk vacancy diffusion coefficient, $D_V = (9 \times 10^{-7}\ \text{m}^2\ \text{s}^{-1}) \exp(-1.95\ \text{eV}/k_BT)$, giving a diffusivity of $5 \times 10^{-18}$ m$^2$ s$^{-1}$ at 600 °C. The activation energy decreases very close to the pyrite surface, resulting in faster vacancy diffusion near the surface than in the bulk (e.g., $E_a$ = 1.5 eV and $D_V = 2 \times 10^{-15}$ m$^2$ s$^{-1}$ near the (100) surface). Using the vacancy formation enthalpy near the surface, the corresponding calculated expression for sulfur-self-diffusion in bulk pyrite is $D_S = (9 \times 10^{-7}\ \text{m}^2\ \text{s}^{-1}) \exp(-2.37\ \text{eV}/k_BT)$, giving a diffusivity of $2 \times 10^{-20}$ m$^2$ s$^{-1}$ at 600 °C. The calculated value of $D_S$ is in good agreement with experiment at intermediate temperatures (~275–625 °C), but the experimental values of $D_0$ and the activation energy for diffusion are substantially smaller than predicted by our model. To eliminate sulfur vacancies in the crystal bulk, pyrite growth and annealing should be performed at elevated temperature in sulfur-rich conditions.

## AUTHOR INFORMATION


### Corresponding Author

*E-mail: yanningz@csrc.ac.cn.


### Notes

The authors declare no competing financial interest.

## ACKNOWLEDGMENTS

We thank the NSF SOLAR Program (Award CHE-1035218), the UCI School of Physical Sciences Center for Solar Energy, and the startup fund of China Thousand Young Talents Program for support of this work. Calculations were performed on parallel computers at NERSC, NSF supercomputer centers, and Tianhe2-JK in the Beijing Computational Science Research Center.

## REFERENCES


(1) Elcock, E. W. Vacancy Diffusion in Ordered Alloys. *Proc. Phys. Soc., London* **1959**, *73*, 250–264.

(2) Van der Ven, A.; Yu, H. C.; Ceder, G.; Thornton, K. Vacancy Mediated Substitutional Diffusion in Binary Crystalline Solids. *Prog. Mater. Sci.* **2010**, *55*, 61–105.

(3) Ho, G.; Ong, M. T.; Caspersen, K. J.; Carter, E. A. Energetics and Kinetics of Vacancy Diffusion and Aggregation in Shocked Aluminium via Orbital-free Density Functional Theory. *Phys. Chem. Chem. Phys.* **2007**, *9*, 4951–4966.

(4) Aschauer, U.; Bowen, P.; Parker, S. C. Oxygen Vacancy Diffusion in Alumina: New Atomistic Simulation Methods Applied to an Old Problem. *Acta Mater.* **2009**, *57*, 4765–4772.

(5) Huang, G. Y.; Wang, C. Y.; Wang, J. T. First-principles Study of Diffusion of Oxygen Vacancies and Interstitials in ZnO. *J. Phys.: Condens. Matter* **2009**, *21*, 195403.

(6) Yoshiya, M.; Oyama, T. Impurity and Vacancy Segregation at Symmetric Tilt Grain Boundaries in YO-doped ZrO. *J. Mater. Sci.* **2011**, *46*, 4176.

(7) Chen, T. J.; Kuo, C. L. First Principles Study of the Oxygen Vacancy Formation and the Induced Defect States in Hafnium Silicates. *J. Appl. Phys.* **2012**, *111*, 074106.

(8) Tang, C.; Tuttle, B.; Ramprasad, R. Diffusion of O Vacancies near Si:$HfO_2$ Interfaces: An ab initio Investigation. *Phys. Rev. B: Condens. Matter Mater. Phys.* **2007**, *76*, 073306.

(9) Tang, C.; Ramprasad, R. Point Defect Chemistry in Amorphous $HfO_2$: Density Functional Theory Calculations. *Phys. Rev. B: Condens. Matter Mater. Phys.* **2010**, *81*, 161201(R).

(10) Geng, W. T.; Freeman, A. J.; Wu, R.; Geller, C. B.; Raynolds, J. E. Embrittling and Strengthening Effects of Hydrogen, Boron, and




DOI: 10.1021/acs.jpcc.5b08300
J. Phys. Chem. C XXXX, XXX, XXX–XXX

Phosphorus on a Σ5 Nickel Grain Boundary. *Phys. Rev. B: Condens. Matter Mater. Phys.* **1999**, *60*, 7149−7155.
(11) Yamaguchi, M.; Shiga, M.; Kaburaki, H. Grain Boundary Decohesion by Impurity Segregation in a Nickel-sulfur System. *Science* **2005**, *307*, 393−397.
(12) Murphy, R.; Strongin, D. R. Surface Reactivity of Pyrite and Related Sulfides. *Surf. Sci. Rep.* **2009**, *64*, 1−45.
(13) Ennaoui, A.; Fiechter, S.; Jaegermann, W.; Tributsch, H. Photoelectrochemistry of Highly Quantum Efficient Single Crystalline *n*-$FeS_2$ (Pyrite). *J. Electrochem. Soc.* **1986**, *133*, 97−106.
(14) Buker, K.; Alonso-Vante, N.; Tributsch, H. Photovoltaic Output Limitation of *n*-$FeS_2$ (pyrite) Schottky Barriers: A Temperature-dependent Characterization. *J. Appl. Phys.* **1992**, *72*, 5721−5728.
(15) Antonuccia, V.; Aricò, A. S.; Giordano, N.; Antonucci, P. L.; Russo, U.; Cocke, D. L.; Crea, F. Photoactive Screen-printed Pyrite Anodes for Electrochemical Photovoltaic Cells. *Sol. Cells* **1991**, *31*, 119−141.
(16) Ennaoui, A.; Fiechter, S.; Pettenkofer, Ch.; Alonso-Vante, N.; Büker, K.; Bronold, M.; Höpfner, Ch.; Tributsch, H. Iron Disulfide for Solar Energy Conversion. *Sol. Energy Mater. Sol. Cells* **1993**, *29*, 289−370.
(17) Bronold, M.; Pettenkofer, C.; Jaegermann, W. Surface Photovoltage Measurements on Pyrite (100) Cleavage Planes: Evidence for Electronic Bulk Eefects. *J. Appl. Phys.* **1994**, *76*, 5800−5808.
(18) Limpinsel, M.; Farhi, N.; Berry, N.; Lindemuth, J.; Perkins, C. L.; Lin, Q.; Law, M. An Inversion Layer at the Surface of n-type Iron Pyrite. *Energy Environ. Sci.* **2014**, *7*, 1974−1989.
(19) Sun, R.; Chan, M. K. Y.; Kang, S. Y.; Ceder, G. Intrinsic Stoichiometry and Oxygen-induced p-type Conductivity of Pyrite $FeS_2$. *Phys. Rev. B: Condens. Matter Mater. Phys.* **2011**, *84*, 035212.
(20) Sun, R.; Ceder, G. Feasibility of Band Gap Engineering of Pyrite $FeS_2$. *Phys. Rev. B: Condens. Matter Mater. Phys.* **2011**, *84*, 245211.
(21) Yu, L. P.; Lany, S.; Kykyneshi, R.; Jieratum, V.; Ravichandran, R.; Pelatt, B.; Altschul, E.; Platt, H. A. S.; Wager, J. F.; Keszler, D. A.; et al. Iron Chalcogenide Photovoltaic Absorbers. *Adv. Energy Mater.* **2011**, *1*, 748−753.
(22) Hu, J.; Zhang, Y. N.; Law, M.; Wu, R. Q. First-principles studies of the electronic properties of native and substitutional anionic defects in bulk iron pyrite. *Phys. Rev. B: Condens. Matter Mater. Phys.* **2012**, *85*, 085203.
(23) Zhang, Y. N.; Hu, J.; Law, M.; Wu, R. Q. Effect of Surface Stoichiometry on the Band Gap of the Pyrite $FeS_2$ (100) Surface. *Phys. Rev. B: Condens. Matter Mater. Phys.* **2012**, *85*, 085314.
(24) Hu, J.; Zhang, Y. N.; Law, M.; Wu, R. Q. Increasing the Band Gap of Iron Pyrite by Alloying with Oxygen. *J. Am. Chem. Soc.* **2012**, *134*, 13216−13219.
(25) Fiechter, S. Defect Formation Energies and Homogeneity Ranges of Rock Salt-, Pyrite-, Chalcopyrite- and Molybdenite-type Compound Semiconductors. *Sol. Energy Mater. Sol. Cells* **2004**, *83*, 459−477.
(26) Krishnamoorthy, A.; Herbert, F. W.; Yip, S.; Van Vliet, K. J.; Yildiz, B. Electronic States of Intrinsic Surface and Bulk Vacancies in $FeS_2$. *J. Phys.: Condens. Matter* **2013**, *25*, 045004.
(27) Birkholz, M.; Fiechter, S.; Hartmann, A.; Tributsch, H. Sulfur Deficiency in Iron Pyrite ($FeS_{2-x}$) and its Consequences for Band-structure Models. *Phys. Rev. B: Condens. Matter Mater. Phys.* **1991**, *43*, 11926−11936.
(28) Jablonski, A.; Wandelt, K. Quantitative Aspects of Ultraviolet Photoemission of Adsorbed Xenon - A Review. *Surf. Interface Anal.* **1991**, *17*, 611−627.
(29) Guevremont, J. M.; Strongin, D. R.; Schoonen, M. A. A. Photoemission of Adsorbed Xenon, X-ray Photoelectron Spectroscopy, and Temperature-Programmed Desorption Studies of $H_2O$ on $FeS_2$(100). *Langmuir* **1998**, *14*, 1361−1366.
(30) Rosso, K. M.; Becker, U.; Hochella, M. F., Jr. Surface Defects and Self-Diffusion on Pyrite {100}: an Ultra High Vacuum Scanning Tunneling Microscopy and Theoretical Modeling Study. *Am. Mineral.* **2000**, *85*, 1428.
(31) Schieck, R.; Hartmann, A.; Fiechter, S.; Könenkamp, R.; Wetzel, H. Electrical Properties of Natural and Synthetic Pyrite ($FeS_2$) Crystals. *J. Mater. Res.* **1990**, *5*, 1567−1572.
(32) Luck, J.; Hartmann, A.; Fiechter, S. Stoichiometry and Impurity Concentration in Synthetically Grown Iron Pyrite Crystals and their Constituents. *Fresenius' Z. Anal. Chem.* **1989**, *334*, 441−446.
(33) Bronold, M.; Tomm, Y.; Jaegermann, W. Surface States on Cubic *d*-band Semiconductor Pyrite ($FeS_2$). *Surf. Sci.* **1994**, *314*, L931−936.
(34) Raybaud, P.; Kresse, G.; Hafner, J.; Toulhoat, H. Ab initio Density Functional Studies of Transition-metal Sulphides: I. Crystal Structure and Cohesive Properties. *J. Phys.: Condens. Matter* **1997**, *9*, 11085.
(35) Raybaud, P.; Kresse, G.; Hafner, J.; Toulhoat, H. Ab initio Density Functional Studies of Transition-metal Sulphides: II. Electronic Structure. *J. Phys.: Condens. Matter* **1997**, *9*, 11107.
(36) Stirling, A.; Bernasconi, M.; Parrinello, M. Defective Pyrite(100) Surface: An Ab initio Study. *Phys. Rev. B: Condens. Matter Mater. Phys.* **2007**, *75*, 165406.
(37) Philpott, M. R.; Goliney, I. Y.; Lin, T. T.; Yu, I. Molecular Dynamics Simulation of Water in a Contact with an Iron Pyrite $FeS_2$ Surface. *J. Chem. Phys.* **2004**, *120*, 1943.
(38) Lehner, S. W.; Newman, N.; van Schilfgaarde, M.; Bandyopadhyay, S.; Savage, K.; Buseck, P. R. Defect Energy Levels and Electronic Behavior of Ni-, Co-, and As-doped Synthetic Pyrite ($FeS_2$). *J. Appl. Phys.* **2012**, *111*, 083717.
(39) Alfonso, D. R. Computational Investigation of $FeS_2$ Surfaces and Prediction of Effects of Sulfur Environment on Stabilities. *J. Phys. Chem. C* **2010**, *114*, 8971.
(40) Fiechter, S.; Mai, J.; Ennaoui, A.; Szacki, W. Chemical vapour transport of pyrite ($FeS_2$) with halogen (Cl, Br, I). *J. Cryst. Growth* **1986**, *78*, 438−444.
(41) Macpherson, H. A.; Stoldt, C. R. Iron Pyrite Nanocubes: Size and Shape Considerations for Photovoltaic Application. *ACS Nano* **2012**, *6*, 8940−8949.
(42) Kirkeminde, A.; Ren, S. Thermodynamic control of iron pyrite nanocrystal synthesis with high photoactivity and stability. *J. Mater. Chem. A* **2013**, *1*, 49−54.
(43) Kresse, G.; Furthmüller, J. Efficiency of Ab-initio Total Energy Calculations for Metals and Semiconductors Using a Plane-wave Basis Set. *Comput. Mater. Sci.* **1996**, *6*, 15−50.
(44) Blöchl, P. E. Projector Augmented-wave Method. *Phys. Rev. B: Condens. Matter Mater. Phys.* **1994**, *50*, 17953−17979.
(45) Perdew, J. P.; Burke, K.; Ernzerhof, M. Generalized Gradient Approximation Made Simple. *Phys. Rev. Lett.* **1996**, *77*, 3865−3868.
(46) Anisimov, V. I.; Aryasetiaswan, F.; Lichtenstein, A. I. First-principles Calculations of the Electronic Structure and Spectra of Strongly Correlated Systems: the LDA+U Method. *J. Phys.: Condens. Matter* **1997**, *9*, 767−808.
(47) Dudarev, S. L.; Botton, G. A.; Savrasov, S. Y.; Humphreys, C. J.; Sutton, A. P. Electron-energy-loss Spectra and the Structural Stability of Nickel Oxide: An LSDA+U Study. *Phys. Rev. B: Condens. Matter Mater. Phys.* **1998**, *57*, 1505−1509.
(48) Berry, N.; Cheng, M.; Perkins, C. L.; Limpinsel, M.; Hemminger, J. C.; Law, M. Atmospheric-Pressure Chemical Vapor Deposition of Iron Pyrite Thin Films. *Adv. Energy Mater.* **2012**, *2*, 1124−1135.
(49) Cabań-Acevedo; Faber, M. S.; Tan, Y. Z.; Hamers, R. J.; Jin, S. Synthesis and Properties of Semiconducting Iron Pyrite ($FeS_2$) Nanowires. *Nano Lett.* **2012**, *12*, 1977−1982.
(50) Barnard, A. S.; Russo, S. P. Shape and Thermodynamic Stability of Pyrite $FeS_2$ Nanocrystals and Nanorods. *J. Phys. Chem. C* **2007**, *111*, 11742−11746.
(51) Vineyard, G. H. Frequency Factors and Isotope Effects in Solid State Rate Processes. *J. Phys. Chem. Solids* **1957**, *3*, 121−127.
(52) Watson, E. B.; Cherniak, D. J.; Frank, E. A. Retention of Biosignatures and Mass-independent Fractionations in Pyrite: Self-diffusion of Sulfur. *Geochim. Cosmochim. Acta* **2009**, *73*, 4792−4802.


DOI: 10.1021/acs.jpcc.5b08300
*J. Phys. Chem. C* XXXX, XXX, XXX−XXX